On the Spatial Error Propagation Characteristics of Cooperative Localization in Wireless Networks

Bingpeng Zhou, Qingchun Chen, *Senior Member, IEEE*, Pei Xiao, *Senior Member, IEEE*, and Lian Zhao, *Senior Member, IEEE*

***Abstract*—Cooperative localization is an important technique in wireless networks. However, there are always errors in network node localization, which will spatially propagate among network nodes when performing network localization. In this paper, we study the spatial error propagation (EP) characteristics of network localization in terms of Fisher information. First, the spatial propagation function is proposed to reveal the spatial cooperation principle of network localization. Second, the convergence property of spatial localization information propagation (SLIP) is analyzed to shed light on the performance limits of network localization through spatial information propagation. It is shown that 1) the network localization error propagates in the way of Ohm's law in electric circuit theory, where the measurement accuracy, node location accuracy, and geometric-resolution information behave like the resistances connected in parallel or series; 2) the network location error gradually diminishes with spatial localization cooperation procedures, due to the cooperative localization information propagation; and 3) the essence of spatial localization cooperation among network nodes is the spatial propagation of localization information.**

***Index Terms*—Error propagation (EP), Fisher information, network localization, spatial cooperation.**

I. Introduction

COOPERATIVE localization plays an important role in wireless networks [1]. It provides effective localization solutions for the location-aware services such as warehousing management, location-aware security, delay-tolerant network routing [2], [3], and shopping mall navigation. It revolutionizes the way people search, locate, and navigate the points of interest inside buildings [4]. The localization security is prerequisite for the localization-aware services. The location privacy might not be as secure as the service provider claimed [5], and the privacy-preserving Wi-Fi localization scheme can be employed to overcome privacy issues [6].

Manuscript received November 29, 2015; revised February 24, 2016; accepted April 7, 2016. Date of publication April 20, 2016; date of current version February 10, 2017. This work was supported in part by the National Natural Science Foundation of China under Grant 61271246, by the National Basic Research Program of China (973 Program) under Grant 2012-CB316100, and by the Royal Academy of Engineering under Award 1314-2. The review of this paper was coordinated by Prof. X. Wang.

B. Zhou and Q. Chen are with Southwest Jiaotong University, Chengdu 610031, China (e-mail: zhoubingpeng@163.com; qcchen@swjtu.edu.cn).

P. Xiao is with University of Surrey, Guildford GU2 7XH, U.K. (e-mail: p.xiao@surrey.ac.uk).

L. Zhao is with Ryerson University, Toronto, ON M5B 2K3, Canada (e-mail: l5zhao@ryerson.ca).

Color versions of one or more of the figures in this paper are available online at http://ieeexplore.ieee.org.

Digital Object Identifier 10.1109/TVT.2016.2555329

Given network measurements, the network nodes can be calibrated with each other, with an expectation to improve their location accuracies. The node calibrated in the previous round can be used to calibrate its neighboring nodes' locations. Hence, we can finally observe a spatial cooperation between a node and other remote nodes, which are outside its sensing coverage. However, due to the limited localization accuracy, there always exist errors in network node locations. Location errors can also be spatially propagated among network nodes in the calibration stage. Hence, the localization error propagation (EP) will become a critical issue in the network localization. Consequently, we seek answers to the following questions in this paper.

- How do localization errors propagate spatially within the localization network?
- What are the performance limits of network localization, given the fixed size of measurements among network nodes?

Since Fisher information upper bounds on the localization accuracy [7], it can be used as an information metric to measure the localization accuracy intensity. Hence, in this paper, we investigate the localization EP and spatial localization cooperation in terms of information propagation.

In principle, if a signal is correlated with the relative geometry between the target and reference objects, it can be used as the measurement data to determine the target location, such as the visual signal (e.g., landmark picture or video) [8], [9]; acoustic signal [10]; wireless radio signal [11] [e.g., time-of-arrival (TOA); received signal strength (RSS); and angle-of-arrival (AOA)], channel state information [12], and optical signal [13]. The wireless localization/tracking performance limits with different measurement modalities in different environments have been studied in previous research efforts. In [14] and [15], the fundamental limits of cooperative/noncooperative localization in wideband wireless networks are investigated to examine the impact of multipath and non-line-of-sight transmission. In [16], the spatial localization cooperation between a node and its neighboring nodes was investigated. In [17], the Cramer–Rao lower bound is presented to benchmark the simultaneous localization and tracking error in wireless sensor networks. The localization performance analysis was presented in [18] to quantify the effects of reference location uncertainties. In [19], information coupling is studied for cooperative localization by means of Fisher information analysis. The navigation information evolution is addressed in [20] to highlight the spatial and temporal cooperation in navigation networks.

The fundamental limit of mobile localization, particularly the temporal propagation of tracking errors, is revealed in [21], where different types of wireless networks measurements and performance requirements in various scenarios are considered.

However, these state-of-the-art solutions assume localization cooperation between a node and its nearby nodes. A few previous analyses considered the localization information propagation between a node and the remote nodes. In particular, it is the general localization/tracking issue addressed in [14]–[21], where the one-step spatial cooperation among nearby nodes is assumed. Nevertheless, the whole localization information propagation, where each node may cooperate with those remote nodes outside its direct sensing range (extensive spatial cooperation), is neglected.

In this paper, the cooperative localization EP within the whole network is studied, which not only unveils the spatial cooperation mechanism of network localization but also provides insights into performance limits of network localization through extensive spatial cooperation. In addition, the analysis on spatial information propagation in this paper is applied to the TOA-, AOA-, and RSS-based localization. The main contributions of this paper are twofold.

- The localization cooperation principle, in the spatial field, is revealed in terms of localization information propagation. It is shown that the network localization EP complies with the Ohm's law in electric circuit theory, where the measurement accuracy, node location accuracy, and geometric-resolution factor behave like the resistances connected in parallel or series.
- The convergence properties and asymptotic performance are analyzed to provide the insights into the performance limits of spatial localization cooperation. Although reference node locations are inaccurate, the localization error of each node can still be reduced statistically, due to the cooperative localization information propagation. It is disclosed that the essence of localization cooperation among network nodes is the spatial propagation of the associated localization information.

The remainder of this paper is organized as follows. Section II presents the system model and problem formulation. The spatial localization information propagation (SLIP) is investigated in Section III. In Section IV, the convergence property of SLIP is analyzed. The asymptotic performance analysis is presented in Section V. Simulations results are presented in Section VI. Finally, Section VII concludes this paper.

II. System Model

Prior to presenting the SLIP analysis in Section III, here, we clarify the system model first.

A. Network Model

A static wireless network is considered in this paper, as shown in Fig. 1, where M network nodes are randomly and uniformly distributed inside the deployment area. Due to the unavoidable acquisition errors in their initial locations, all node locations are inaccurate. The true (but unknown) location of the ith network node is denoted by a D-dimensional column vector $\mathbf{s}_i$, whereas the coarse location (inaccurate location with a precision $\mathbf{U}_i$) is denoted by $\boldsymbol{\mu}_i$.[1] Generally, the true location $\mathbf{s}_i$ is modeled as a Gaussian variable with the center $\boldsymbol{\mu}_i$ and the precision $\mathbf{U}_i$, namely

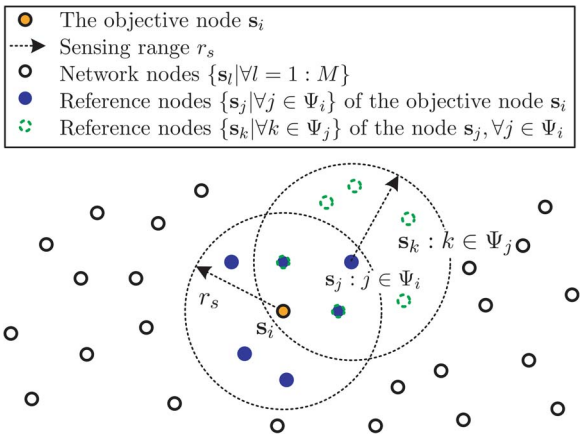

Fig. 1. Network node deployment.

$$\mathbf{s}_i \sim \mathcal{N}(\mathbf{s}_i|\boldsymbol{\mu}_i, \mathbf{U}_i) \qquad \forall\, i = 1:M \tag{1}$$

where we assume node location precision $\mathbf{U}_i$ is independent to others since the measurements and location estimations of different nodes are independent from each other [22], [23]. The location uncertainty is defined as the inverse of the location precision matrix $\mathbf{U}_i$.

This model can subsume the case where a certain node location is completely unknown when its precision $\mathbf{U}_i \to \mathbf{0}$. On the other hand, there is no anchor node assumed inside the whole area, and all nodes are to be located with the cooperation of other nodes. However, when $\mathbf{U}_i$ is sufficiently large, node $\mathbf{s}_i$ is equivalent to the anchor node with precisely known location.

Considering the localization of node $\mathbf{s}_i$ (the objective node), we assume $\mathbf{s}_i$ is within the sensing range r_s of M_i nearby nodes (reference nodes), and we define the index set of these reference nodes as

$$\Psi_i \doteq \left\{j : \|\mathbf{s}_j - \mathbf{s}_i\|_2 < r_s \qquad \forall\, j \neq i\right\} \tag{2}$$

where $\|\bullet\|_2$ denotes the ℓ_2-norm on the vector. Hence, we have that $|\Psi_i| = M_i$, where $|\bullet|$ stands for the set size. We assume these reference nodes report their coarse locations and precision $\{\boldsymbol{\mu}_j, \mathbf{U}_j : \forall\, j \in \Psi_i\}$ to the objective node $\mathbf{s}_i$ to cooperatively localize it.

B. Measurement Model

The measurement model of cooperative wireless localization (incorporating the location information of nodes $\mathbf{s}_i$ and $\mathbf{s}_j$) is generalized as

$$z_{i,j} = h(\mathbf{s}_i, \mathbf{s}_j) + \epsilon_{i,j} \qquad \forall\, j \in \Psi_i \text{ and } \forall\, i = 1:M \tag{3}$$

[1]The coarse location $\boldsymbol{\mu}_i$ and its precision matrix $\mathbf{U}_i$ can be derived from the previous cooperative positioning rounds, which are recorded by the node itself and will be reported to its neighbor node (the objective node to be localized) in the next positioning round.

where the scalar $z_{i,j}$ denotes the measurement from $\mathbf{s}_j$ to $\mathbf{s}_i$, and $\epsilon_{i,j}$ represents the measurement noise, which is generally assumed Gaussian with zero-mean and precision ω, namely, $\epsilon_{i,j} \sim \mathcal{N}(\epsilon_{i,j}|0,\omega)$.[2] In particular, $h(\mathbf{s}_i,\mathbf{s}_j)$ is defined as the measurement function that depends on the distance $\|\mathbf{s}_i-\mathbf{s}_j\|_2$ (for the range-based methods) [21], the angle $\angle(\mathbf{s}_i,\mathbf{s}_j)$ (for the direction-based methods) [16], or the connectivity $\mathcal{C}(\mathbf{s}_i,\mathbf{s}_j)$ [27] of two nodes.

In this paper, the SLIP analysis is valid for the TOA [15], RSS [17], [28], and AOA-based localization [29], [30], where the associated measurement function $h(\mathbf{s}_i,\mathbf{s}_j)$ can be specified, respectively, as[3] [21]

$$h_{\mathrm{TOA}}(\mathbf{s}_i,\mathbf{s}_j) = \|\mathbf{s}_i-\mathbf{s}_j\|_2 \tag{4}$$

$$h_{\mathrm{RSS}}(\mathbf{s}_i,\mathbf{s}_j) = \phi - 10\gamma\log_{10}\|\mathbf{s}_i-\mathbf{s}_j\|_2 \tag{5}$$

$$h_{\mathrm{AOA}}(\mathbf{s}_i,\mathbf{s}_j) = \varphi_j + \frac{180}{\pi}\mathrm{actan}\left(\frac{[\mathbf{s}_i-\mathbf{s}_j]_2}{[\mathbf{s}_i-\mathbf{s}_j]_1}\right) \tag{6}$$

wherein $\phi = P_T - L_0 + 10\gamma\log_{10} d_0$ and P_T is the transmit power, L_0 denotes the path loss associated with the reference distance d_0, and γ denotes the path-loss exponent [31]. In addition, $[\mathbf{x}]_k$ stands for the kth $(k=1,2)$ element of a 2-D vector $\mathbf{x}$, and φ_j stands for the direction of the antenna main lobe. Unless otherwise stated, we use $h(\mathbf{s}_i,\mathbf{s}_j)$ to denote the general range-based measurement functions.

C. Statistical Model

Let $\boldsymbol{c}_i = \mathrm{vec}[\mathbf{s}_j]_{\forall\, j\in\Psi_i}$ denote the vector of reference node set, where $\mathrm{vec}[\bullet_j]_{\forall\, j\in\Psi_i}$ yields a column vector stacked by all components $\{\bullet_j : \forall\, j\in\Psi_i\}$. Consider the positioning of node $\mathbf{s}_i$ (the objective node), and we define an $(M_i+1)D$-dimensional complete variable as $\boldsymbol{\alpha}_i := \begin{bmatrix}\mathbf{s}_i\\ \boldsymbol{c}_i\end{bmatrix}$. All measurements of $\mathbf{s}_i$ from $\boldsymbol{c}_i$ is stacked as $\mathbf{z}_i = \mathrm{vec}[z_{i,j}]_{\forall\, j\in\Psi_i}$.

By assuming the measurements conditioned on $\mathbf{s}_i$ are mutually independent, the likelihood distribution is cast as

$$p(\mathbf{z}_i|\mathbf{s}_i,\mathbf{s}_j) = \prod_{j\in\Psi_i}\frac{|\omega|^{\frac{1}{2}}}{\sqrt{2\pi}}\exp\left(-\frac{1}{2}\omega\left(z_{i,j}-h(\mathbf{s}_i,\mathbf{s}_j)\right)^2\right)$$

where $|\omega|$ stands for the absolute value of precision ω.

Hence, the *a posteriori* distribution can be written as

$$\begin{aligned} p(\boldsymbol{\alpha}_i|\mathbf{z}_i) &\propto p(\mathbf{z}_i|\boldsymbol{\alpha}_i)p(\boldsymbol{\alpha}_i)\\ &= \prod_{j\in\Psi_i}\frac{|\omega|^{\frac{1}{2}}}{\sqrt{2\pi}}\exp\left(-\frac{1}{2}\omega\left(z_{i,j}-h(\mathbf{s}_i,\mathbf{s}_j)\right)^2\right)\\ &\quad\cdot\mathcal{N}(\mathbf{s}_i|\boldsymbol{\mu}_i,\mathbf{U}_i)\mathcal{N}(\mathbf{s}_j|\boldsymbol{\mu}_j,\mathbf{U}_j) \end{aligned} \tag{7}$$

where $\propto$ implies the left term is proportional to the right.

[2]For the TOA-based localization, we have considered the case that the non-light-of-sight signal can be identified and removed by the identification methods [24], [25] and its positive ranging error can also be mitigated [26]. The network timer is also assumed synchronized.

[3]For the AOA-based localization [see (6)], we assume the scenario is in a 2-D Euclidean space, i.e., $D=2$.

D. Problem Formulation

By localization cooperation, the network nodes could improve their location accuracy. However, the *a priori* location errors and localization errors can be propagated among network nodes. In view of this, we aim to address the following issues.

- How does the localization information spatially propagate among inaccurate network nodes?
- Given the coarse locations and the precision parameters $\{\boldsymbol{\mu}_i,\mathbf{U}_i|\forall\, i=1:M\}$ of network nodes and measurements $\{z_{i,j}|\forall\, j\in\Psi_i,\forall\, i=1:M\}$, what are the performance limits of node location calibration?

III. Spatial Localization Cooperation

Here, we study the spatial localization cooperation in a perspective of localization information propagation.

A. Localization Information

In the parameter estimation theory, for an unbiased Bayesian estimation (BE) of a nondeterministic variable $\boldsymbol{\alpha}_i$, the covariance matrix of estimation error is lower bounded by a Cramer–Rao lower bound (CRLB) [28] (which is denoted by $\boldsymbol{\mathcal{B}}_{\mathrm{BE}}(\boldsymbol{\alpha}_i)$ in this paper), as follows:

$$\mathrm{cov}(\widehat{\boldsymbol{\alpha}}_i) \succeq \boldsymbol{\mathcal{B}}_{\mathrm{BE}}(\boldsymbol{\alpha}_i) \tag{8}$$

where the CRLB $\boldsymbol{\mathcal{B}}_{\mathrm{BE}}(\boldsymbol{\alpha}_i)$ is calculated as the inverse of a Fisher information matrix (FIM). We define the localization accuracy (or precision) as the inverse of the error covariance matrix. The Fisher information is defined as [7]

$$\boldsymbol{\mathcal{I}}_{\mathrm{BE}}(\boldsymbol{\alpha}_i) = -\mathbb{E}_{\boldsymbol{\alpha}_i,\mathbf{z}_i}\left\{\nabla_{\boldsymbol{\alpha}_i,\boldsymbol{\alpha}_i^\top}\ln p(\boldsymbol{\alpha}_i|\mathbf{z}_i)\right\} \tag{9}$$

where the operator $\mathbb{E}_{\boldsymbol{\alpha}_i,\mathbf{z}_i}\{\bullet\}$ denotes the expectation with respect to the distribution $p(\boldsymbol{\alpha}_i,\mathbf{z}_i)$, and $\nabla_{\boldsymbol{\alpha}_i,\boldsymbol{\alpha}_i^\top}$ denotes the second-order derivative.

Based on the given formulation we can see that the FIM can be considered as the upper bound of localization accuracy. Hence, it can be used as a localization performance metric that measures the supremum of localization accuracy. In this paper, we investigate the spatial cooperation of wireless localization and the spatial propagation of localization information in terms of Fisher information analysis.

We now calculate the full Bayesian localization information matrix of node $\mathbf{s}_i$ (regarded as the objective node). Suppose that the M_i reference nodes of node $\mathbf{s}_i$ are successively labeled by $\mathbf{s}_1,\ldots,\mathbf{s}_{M_i}$. Assume variables $\mathbf{s}_i$ and $\mathbf{s}_j$ $(\forall\, i\neq j)$ are *priori* independent. According to (9), its full information matrix $\boldsymbol{\mathcal{I}}_{\mathrm{BE}}(\boldsymbol{\alpha}_i)$ can be structured as (10), shown at the bottom of the next page, where we utilize the fact that $\boldsymbol{\mathcal{I}}_{\mathrm{BE}}(\mathbf{s}_i,\mathbf{s}_j) = \boldsymbol{\mathcal{I}}_{\mathrm{MLE}}(\mathbf{s}_i,\mathbf{s}_j) + \delta_{i,j}\boldsymbol{\mathcal{I}}_P(\mathbf{s}_i)$, whereas $\boldsymbol{\mathcal{I}}_{\mathrm{MLE}}(\mathbf{s}_i,\mathbf{s}_j)$ and $\boldsymbol{\mathcal{I}}_P(\mathbf{s}_i)$ denote the maximum likelihood estimation (MLE)-based information (from the measurement only) and the *a priori* information, respectively. Here, $\delta_{i,j}=1$ if $i=j$, and zero otherwise.

The generic information intensities $\boldsymbol{\mathcal{I}}_{\mathrm{MLE}}(\mathbf{s}_i,\mathbf{s}_j)$ and $\boldsymbol{\mathcal{I}}_P(\mathbf{s}_i)$ in (10) are specified as

$$\boldsymbol{\mathcal{I}}_{\mathrm{MLE}}(\mathbf{s}_i,\mathbf{s}_i)=\sum_{j\in\Psi_i}\omega\mathbf{A}_{i,j} \tag{11}$$

$$\boldsymbol{\mathcal{I}}_P(\mathbf{s}_i)=\mathbf{U}_i \tag{12}$$

$$\boldsymbol{\mathcal{I}}_{\mathrm{MLE}}(\mathbf{s}_i,\mathbf{s}_j)=-\omega\mathbf{A}_{i,j}\qquad \forall\, j\in\Psi_i \tag{13}$$

$$\boldsymbol{\mathcal{I}}_{\mathrm{MLE}}(\mathbf{s}_j,\mathbf{s}_j)=\omega\mathbf{A}_{i,j}\qquad \forall\, j\in\Psi_i \tag{14}$$

$$\boldsymbol{\mathcal{I}}_P(\mathbf{s}_j)=\mathbf{U}_j\qquad \forall\, j\in\Psi_i \tag{15}$$

$$\boldsymbol{\mathcal{I}}_{\mathrm{MLE}}(\mathbf{s}_j,\mathbf{s}_k)=\mathbf{0}\qquad \forall\, j\neq k,\ \text{and}\ j,k\in\Psi_i \tag{16}$$

where $\mathbf{A}_{i,j}$ denotes the geometric resolution metric,[4] which is given, based on three measurement methodologies, by

$$\begin{aligned}\mathbf{A}_{i,j}&=\mathbb{E}_{\mathbf{s}_i,\mathbf{s}_j}\left\{\nabla_{\mathbf{s}_i}h(\mathbf{s}_i,\mathbf{s}_j)\nabla_{\mathbf{s}_i^\top}h(\mathbf{s}_i,\mathbf{s}_j)\right\} \\ &=\begin{cases}\left(\frac{10\gamma}{\ln 10}\right)^2\mathbb{E}_{\mathbf{s}_i,\mathbf{s}_j}\left\{\frac{(\mathbf{s}_i-\mathbf{s}_j)(\mathbf{s}_i-\mathbf{s}_j)^\top}{\|\mathbf{s}_i-\mathbf{s}_j\|_2^4}\right\}, & \text{RSS}\\ \mathbb{E}_{\mathbf{s}_i,\mathbf{s}_j}\left\{\frac{(\mathbf{s}_i-\mathbf{s}_j)(\mathbf{s}_i-\mathbf{s}_j)^\top}{\|\mathbf{s}_i-\mathbf{s}_j\|_2^2}\right\}, & \text{TOA}\\ \left(\frac{180}{\pi}\right)^2\mathbb{E}_{\mathbf{s}_i,\mathbf{s}_j}\left\{\frac{\mathbf{v}_{i,j}\mathbf{v}_{i,j}^\top}{\|\mathbf{s}_i-\mathbf{s}_j\|_2^4}\right\}, & \text{AOA}\end{cases}\end{aligned} \tag{17}$$

$$\mathbf{v}_{i,j}=\begin{bmatrix}[\mathbf{s}_j]_2-[\mathbf{s}_i]_2\\ [\mathbf{s}_i]_1-[\mathbf{s}_j]_1\end{bmatrix}\ \text{(supposing } D=2) \tag{18}$$

where $\mathbf{A}_{i,j}=\mathbf{A}_{j,i}$ and both are symmetric and have full rank. The Bayesian information matrix of its localization is fully formulated by a $(|\Psi_i|+1)D$-dimensional positive semi-definite matrix $\boldsymbol{\mathcal{I}}_{\mathrm{BE}}(\boldsymbol{\alpha}_i)$, which is calculated as (10)–(16).

We now focus on the actual localization accuracy of node $\mathbf{s}_i$, given the inaccurate locations $\{\mathbf{s}_j:\forall\, j\in\Psi_i\}$ of all of its reference nodes. Based on the following information matrix partition [also shown in (10)]:

$$\boldsymbol{\mathcal{I}}_{\mathrm{BE}}(\mathbf{s}_i)=\begin{bmatrix}\boldsymbol{\mathcal{I}}_{\mathrm{BE}}(\mathbf{s}_i,\mathbf{s}_i) & \boldsymbol{\Phi}_{\mathrm{BE}}^\top(\mathbf{s}_i)\\ \boldsymbol{\Phi}_{\mathrm{BE}}(\mathbf{s}_i) & \boldsymbol{\mathcal{R}}_{\mathrm{BE}}(\mathbf{s}_i)\end{bmatrix} \tag{19}$$

where $\boldsymbol{\mathcal{I}}_{\mathrm{BE}}(\mathbf{s}_i,\mathbf{s}_i)=\boldsymbol{\mathcal{I}}_{\mathrm{MLE}}(\mathbf{s}_i,\mathbf{s}_i)+\boldsymbol{\mathcal{I}}_P(\mathbf{s}_i)$, the equivalent information $\boldsymbol{\mathcal{I}}_{\mathrm{EQ}}(\mathbf{s}_i)$ associated with $\mathbf{s}_i$ can be derived by using

[4]Geometric resolution implies the capability that a localization algorithm recognizes the location difference, given certain measurement change.

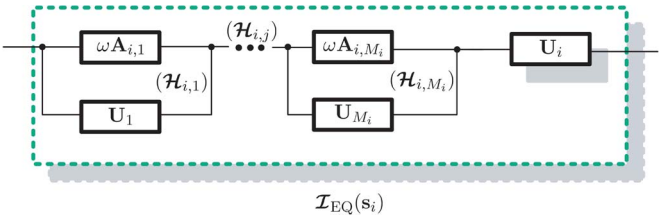

Fig. 2. Spatial propagation of localization information.

Schur's complement as

$$\begin{aligned}\boldsymbol{\mathcal{I}}_{\mathrm{EQ}}(\mathbf{s}_i)&=\boldsymbol{\mathcal{I}}_{\mathrm{BE}}(\mathbf{s}_i,\mathbf{s}_i)-\boldsymbol{\Phi}_{\mathrm{BE}}^\top(\mathbf{s}_i)\left(\boldsymbol{\mathcal{R}}_{\mathrm{BE}}(\mathbf{s}_i)\right)^{-1}\boldsymbol{\Phi}_{\mathrm{BE}}(\mathbf{s}_i)\\ &=\sum_{j\in\Psi_i}\underbrace{\left((\omega\mathbf{A}_{i,j})^{-1}+\mathbf{U}_j^{-1}\right)^{-1}}_{\boldsymbol{\mathcal{H}}_{i,j}}+\mathbf{U}_i\end{aligned} \tag{20}$$

where $\boldsymbol{\mathcal{H}}_{i,j}$ is defined as the equivalent measurement information with reference node location errors.

The detailed derivation can be found in Appendix A. The equivalent information $\boldsymbol{\mathcal{I}}_{\mathrm{EQ}}(\mathbf{s}_i)$ retains all necessary information of localization from its full Bayesian information $\boldsymbol{\mathcal{I}}_{\mathrm{BE}}(\boldsymbol{\alpha}_i)$ in (10), in a term of $[(\boldsymbol{\mathcal{I}}_{\mathrm{BE}}(\boldsymbol{\alpha}_i))^{-1}]_{[1:D,1:D]}=(\boldsymbol{\mathcal{I}}_{\mathrm{EQ}}(\mathbf{s}_i))^{-1}$ [15].

We can see that, the final localization precision relies on the following information factors, i.e., the measurement precision ω, the reference node location precision $\mathbf{U}_j$, the geometric-resolution information $\mathbf{A}_{i,j}$, and the *a priori* location precision $\mathbf{U}_i$. The crude measurement information (disregarding reference node location errors) is defined as $\omega\mathbf{A}_{i,j}$. In principle, the localization performance depends on the measurement size, the density of independent reference sources, *a priori* information, the geometric resolution of measurement methodology, and the measurement noise intensity.

As shown in Fig. 2, all of these localization information factors ($\{\omega\mathbf{A}_{i,j},\mathbf{U}_j:\forall\, j\in\Psi_i\}$ and $\mathbf{U}_i$) propagate like the resistances connected in serial or parallel, which complies with the Ohm's law in electric circuit theory. For the localization of node $\mathbf{s}_i$, the (crude) measurement information $\omega\mathbf{A}_{i,j}$ and location precision $\mathbf{U}_j$ of one reference node $\mathbf{s}_j$ can be deemed as resistances connected in parallel, forming the equivalent measurement information $\boldsymbol{\mathcal{H}}_{i,j}$ (i.e., $R_1=(R_{1,1}^{-1}+R_{1,2}^{-1})^{-1}$ where R_1 stands for the equivalent resistance of two parallel-connected resistances $R_{1,1}$ and $R_{1,2}$); these equivalent measurement information $\{\boldsymbol{\mathcal{H}}_{i,j}:\forall\, j\in\Psi_i\}$ from all reference nodes and itself *a priori* location precision $\mathbf{U}_i$ propagate like the resistances connected in series (resistance summation), forming the final localization information $\boldsymbol{\mathcal{I}}_{\mathrm{EQ}}(\mathbf{s}_i)$ of $\mathbf{s}_i$.

$$\boldsymbol{\mathcal{I}}_{\mathrm{BE}}(\boldsymbol{\alpha}_i)=\left[\begin{array}{c|ccc}\boldsymbol{\mathcal{I}}_{\mathrm{MLE}}(\mathbf{s}_i,\mathbf{s}_i)+\boldsymbol{\mathcal{I}}_P(\mathbf{s}_i) & \boldsymbol{\mathcal{I}}_{\mathrm{MLE}}(\mathbf{s}_i,\mathbf{s}_1) & \cdots & \boldsymbol{\mathcal{I}}_{\mathrm{MLE}}(\mathbf{s}_i,\mathbf{s}_{M_i})\\ \hline \boldsymbol{\mathcal{I}}_{\mathrm{MLE}}(\mathbf{s}_1,\mathbf{s}_i) & \boldsymbol{\mathcal{I}}_{\mathrm{MLE}}(\mathbf{s}_1,\mathbf{s}_1)+\boldsymbol{\mathcal{I}}_P(\mathbf{s}_1) & \cdots & \boldsymbol{\mathcal{I}}_{\mathrm{MLE}}(\mathbf{s}_1,\mathbf{s}_{M_i})\\ \vdots & \vdots & \ddots & \vdots\\ \boldsymbol{\mathcal{I}}_{\mathrm{MLE}}(\mathbf{s}_{M_i},\mathbf{s}_i) & \boldsymbol{\mathcal{I}}_{\mathrm{MLE}}(\mathbf{s}_{M_i},\mathbf{s}_1) & \cdots & \boldsymbol{\mathcal{I}}_{\mathrm{MLE}}(\mathbf{s}_{M_i},\mathbf{s}_{M_i})+\boldsymbol{\mathcal{I}}_P(\mathbf{s}_{M_i})\end{array}\right] \tag{10}$$

$\boldsymbol{\Phi}_{\mathrm{BE}}(\mathbf{s}_i)$ $\quad$ $\boldsymbol{\mathcal{R}}_{\mathrm{BE}}(\mathbf{s}_i)$

B. Spatial Propagation

The localization information in (20) characterizes the initial localization accuracy of the objective node (in the first round of localization), where it has been assumed that the location accuracy of each reference node is the *priori* precision $\mathbf{U}_j, \forall\, j \in \Psi_i$. However, when all network nodes have been mutually localization more than once (here we have assumed a fixed measurement set), the location precision of its reference node is no longer the initial value $\mathbf{U}_j$, but the localization accuracy $\boldsymbol{\mathcal{I}}_{\mathrm{EQ}}(\mathbf{s}_j)$ of the last round. Suppose that, at the nth round of localization, the location accuracy of its reference node $\mathbf{s}_j$ is denoted by $\boldsymbol{\mathcal{I}}^{(n)}_{\mathrm{EQ}}(\mathbf{s}_j)$ $(\forall\, j \in \Psi_i)$, then the localization information of the objective node (at the current localization round) is rewritten as

$$\boldsymbol{\mathcal{I}}^{(n)}_{\mathrm{EQ}}(\mathbf{s}_i) = \sum_{j\in\Psi_i}\left((\omega\mathbf{A}_{i,j})^{-1} + \left(\boldsymbol{\mathcal{I}}^{(n)}_{\mathrm{EQ}}(\mathbf{s}_j)\right)^{-1}\right)^{-1} + \mathbf{U}_i$$

where the localization information of its reference node $\mathbf{s}_j$ can also be similarly expressed by

$$\boldsymbol{\mathcal{I}}^{(n)}_{\mathrm{EQ}}(\mathbf{s}_j) = \sum_{k\in\Psi_j\setminus i}\underbrace{\left((\omega\mathbf{A}_{j,k})^{-1} + \left(\boldsymbol{\mathcal{I}}^{(n)}_{\mathrm{EQ}}(\mathbf{s}_k)\right)^{-1}\right)^{-1}}_{\boldsymbol{\mathcal{H}}^{(n)}_{j,k}} + \left((\omega\mathbf{A}_{j,i})^{-1} + \left(\boldsymbol{\mathcal{I}}^{(n-1)}_{\mathrm{EQ}}(\mathbf{s}_i)\right)^{-1}\right)^{-1} + \mathbf{U}_j \quad (21)$$

where "\" denotes set minus, and $\boldsymbol{\mathcal{H}}^{(n)}_{j,k}$ denotes the equivalent measurement information from node $\mathbf{s}_k$ to node $\mathbf{s}_j$, in the nth localization round. By substituting (21) into (20), the localization information of $\mathbf{s}_i$ can be further written as (22),[5] shown at the bottom of the page, where the measurement information $\boldsymbol{\mathcal{H}}^{(n)}_{j,k}$ is cast as

$$\boldsymbol{\mathcal{H}}^{(n)}_{j,k} = \left((\omega\mathbf{A}_{j,k})^{-1} + \left(\boldsymbol{\mathcal{I}}^{(n)}_{\mathrm{EQ}}(\mathbf{s}_k)\right)^{-1}\right)^{-1} \qquad \forall\, k \in \Psi_j \setminus i. \quad (23)$$

Equation (22) describes a spatial propagation of the localization information among all network nodes. Prior to the discussion of its underlying mechanism, we first introduce some necessary definitions as follows.

[5]We suppose that there is no measurement of $\mathbf{s}_k$ from $\mathbf{s}_i$, namely, $i \notin \Psi_k$ where $k \in \Psi_j$ and $j \in \Psi_i$. In other words, $k \notin \Psi_i \bigcap \Psi_j$.

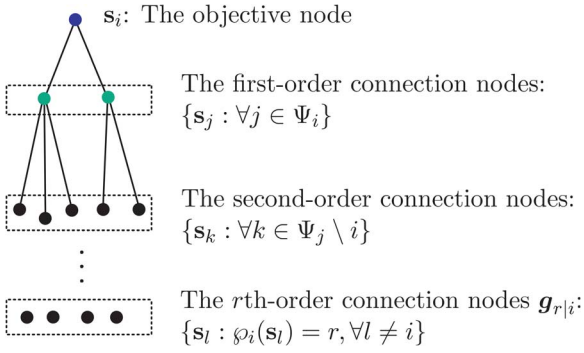

Fig. 3. Network nodes classification according to its connection order $\wp_i$ to the objective node $\mathbf{s}_i$.

Definition 1—(The rth-Order Connection Set $\boldsymbol{g}_{r|i}$): If $\wp_i(\mathbf{s}_l) = r$, we say that the node $\mathbf{s}_l$ belongs to the rth-order connection set of node $\mathbf{s}_i$, which is defined as

$$\boldsymbol{g}_{r|i} = \{\mathbf{s}_l : \wp_i(\mathbf{s}_l) = r\, \forall\, l \neq i\} \quad (24)$$

where $\wp_i(s_l)$ denotes the minimum hops that $\mathbf{s}_l$ connects (in the sense of localization observation) to the node $\mathbf{s}_i$.

$\wp_i(s_l)$ is also referred to as the connection order in the following. In addition, if there is no observation connections from $\mathbf{s}_l$ to $\mathbf{s}_i$, we denote $\wp_i(s_l) = \infty$. In view of this, the reference nodes in Ψ_i of the objective node $\mathbf{s}_i$ is equivalent to its first-order connection set $\boldsymbol{g}_{1|i}$. An example of a connection tree with respect to the objective node $\mathbf{s}_i$, according to the connection orders of network nodes, is shown in Fig. 3. All nodes can be classified accordingly as $\boldsymbol{g}_{1|i}, \boldsymbol{g}_{2|i}, \ldots$. Considering the case of whole network, a connection graph can be finally figured out, and the reference cluster size $|\Psi_i|$ of a generic node $\mathbf{s}_i$ can also be read as its connection multiplicity.

Theorem 1: A node $\mathbf{s}_l$ can contribute to the localization of another node $\mathbf{s}_i$ through spatial cooperation, only if its connection order $\wp_i(s_l) < \infty$ holds, namely, there exists a connection link from $\mathbf{s}_l$ to $\mathbf{s}_i$.

Proof: The reasonableness of Theorem 1 lies in the localization information propagation (22). If $\wp_i(s_l) < \infty$, then there must be a connection link to make the equivalent measurement information $\boldsymbol{\mathcal{H}}^{(n)}_{j,k}$ of the second-order connection nodes to be not lower than zero, namely $\boldsymbol{\mathcal{H}}^{(n)}_{j,k} \succeq \mathbf{0}\ \forall\, j \in \Psi_i$. Hence, its localization accuracy information $\boldsymbol{\mathcal{I}}^{(n)}_{\mathrm{EQ}}(\mathbf{s}_l)$ can finally propagate to the objective node $\mathbf{s}_i$, thus to improve the localization accuracy $\boldsymbol{\mathcal{I}}^{(n)}_{\mathrm{EQ}}(\mathbf{s}_i)$ of node $\mathbf{s}_i$. ■

The remote node $\mathbf{s}_k$ can also contribute to the localization of node $\mathbf{s}_i$ through the spatial propagation of localization

$$\boldsymbol{\mathcal{I}}^{(n)}_{\mathrm{EQ}}(\mathbf{s}_i) = \sum_{j\in\Psi_i}\left((\omega\mathbf{A}_{i,j})^{-1} + \left(\sum_{k\in\Psi_j\setminus i}\boldsymbol{\mathcal{H}}^{(n)}_{j,k} + \underbrace{\left((\omega\mathbf{A}_{j,i})^{-1} + \left(\boldsymbol{\mathcal{I}}^{(n-1)}_{\mathrm{EQ}}(\mathbf{s}_i)\right)^{-1}\right)^{-1}}_{\boldsymbol{\mathcal{H}}^{(n-1)}_{j,i}} + \mathbf{U}_j\right)^{-1}\right)^{-1} + \mathbf{U}_i \quad (22)$$

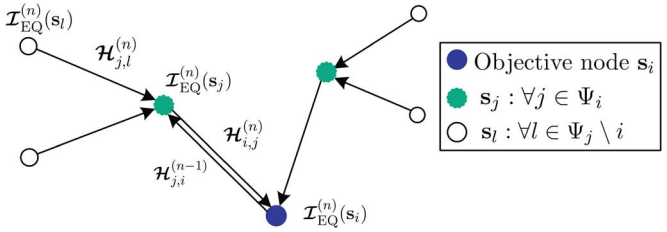

Fig. 4. Spatial propagation of localization information from nodes with various connection orders to the objective node $\mathbf{s}_i$.

information $\mathcal{I}^{(n)}_{\mathrm{BE}}(\mathbf{s}_k) \to \mathcal{I}^{(n)}_{\mathrm{BE}}(\mathbf{s}_j) \to \mathcal{I}^{(n)}_{\mathrm{BE}}(\mathbf{s}_i)$,[6] although it is out of the sensing area of the objective node $\mathbf{s}_i$ (namely, $k \notin \Psi_i$). A simple case of connection network is shown in Fig. 4, where the spatial localization information propagates according to (22). By passing the equivalent measurement information $\boldsymbol{\mathcal{H}}^{(n)}_{j,k}$ through those nodes with each connection order, the objective node $\mathbf{s}_i$ incorporates the localization information $\mathcal{I}^{(n)}_{\mathrm{EQ}}(\mathbf{s}_j)$ and $\mathcal{I}^{(n)}_{\mathrm{EQ}}(\mathbf{s}_k)$ $\forall\, j,k \neq i$, and the last localization information $\mathcal{I}^{(n-1)}_{\mathrm{EQ}}(\mathbf{s}_i)$ of its own. As shown in (22), the term $\boldsymbol{\mathcal{H}}_{j,k}$ ($\forall\, j \in \Psi_i$ and $\forall\, k \in \Psi_j \setminus i$) opens a gate that allows the localization information from the remote nodes $\boldsymbol{g}_{r|i}$ ($\forall\, r \geq 2$) to come into $\mathcal{I}_{\mathrm{EQ}}(\mathbf{s}_i)$. Hence, the localization contribution of a remote node $\mathbf{s}_l$ to $\mathbf{s}_i$ depends on its equivalent measurement information $\boldsymbol{\mathcal{H}}_{l,m}$ $\forall\, m \in \Psi_l$, and its connection order $\wp_i(\mathbf{s}_l)$ to $\mathbf{s}_i$. In addition, the localization accuracy of $\mathbf{s}_i$ depends on its connection multiplicity $|\Psi_i|$.

IV. Convergence Analysis

Here, we will analyze SLIP convergence, which will shed light on the network localization performance limits.

A. SLIP Convergence

Theorem 2: Given the information $\{\boldsymbol{\mu}_i, \mathbf{U}_i : \forall\, i = 1 : M\}$ of all node locations and measurements $\{z_{i,j} : \forall\, i,j\}$, each node location accuracy $\mathcal{I}_{\mathrm{EQ}}(\mathbf{s}_i)$ can converge to an upper state $\mathcal{I}^{\star}_{\mathrm{EQ}}(\mathbf{s}_i)$ through spatial localization cooperation. All node location accuracy $\{\mathcal{I}^{\star}_{\mathrm{EQ}}(\mathbf{s}_i) : \forall\, i\}$ will reach a balance state until there are additional measurements.

Proof: The associated proof is given in Appendix B. ■

The balance state of localization information propagation represents the final accuracy of node localization. Theorem 2 tells us that, although all node locations are not accurate (which means the reference node locations are also inaccurate in the context of cooperative network calibration), given network measurements, each node location accuracy can be improved statistically, through spatial localization cooperation. Namely, there always exists valuable localization information to be exploited even for an inaccurate reference node.

In the following, we aim at analyzing its balancing process through spatial cooperation and finding out its balance state. We can see from (22) that, due to the presence of $\boldsymbol{\mathcal{H}}_{j,k}$, $\forall\, j \in \Psi_i$ and $\forall\, k \in \Psi_j \setminus i$, the localization information of its remote nodes $\boldsymbol{g}_{r|i}, (\forall\, r \in \mathbb{N}_+)$ can determine the balance state $\mathcal{I}_{\mathrm{EQ}}(\mathbf{s}_i)$. The SLIP balance state of any node is jointly determined by $\boldsymbol{\mathcal{H}}_{j,k}$ of other connecting nodes. Let $\mathcal{I}^{\star}_{\mathrm{EQ}}(\mathbf{s}_i)$ denote the SLIP balance state of node $\mathbf{s}_i$ $\forall\, i = 1 : M$, then the balance states of all nodes are the solutions to the joint balance equations in the following:

$$\begin{cases} \mathcal{I}^{\star}_{\mathrm{EQ}}(\mathbf{s}_i) = \sum\limits_{j \in \Psi_i} \boldsymbol{\mathcal{H}}^{\star}_{i,j} + \mathbf{U}_i \\ \mathcal{I}^{\star}_{\mathrm{EQ}}(\mathbf{s}_j) = \sum\limits_{k \in \Psi_j} \boldsymbol{\mathcal{H}}^{\star}_{j,k} + \mathbf{U}_j \\ \quad \vdots \text{ (for all of the rest nodes)} \end{cases} \tag{25}$$

where $\boldsymbol{\mathcal{H}}^{\star}_{i,j}$ denotes the equivalent measurement information with respect to the balanced localization information $\mathcal{I}^{\star}_{\mathrm{EQ}}(\mathbf{s}_j)$ of $\mathbf{s}_j$ $\forall\, j \in \Psi_i$, which is expressed as

$$\boldsymbol{\mathcal{H}}^{\star}_{i,j} = \left((\omega \mathbf{A}_{i,j})^{-1} + \left(\mathcal{I}^{\star}_{\mathrm{EQ}}(\mathbf{s}_j) \right)^{-1} \right)^{-1} \tag{26}$$

and so is $\boldsymbol{\mathcal{H}}^{\star}_{j,k}$. The corresponding localization information gain from spatial propagation is defined as

$$\begin{aligned} \boldsymbol{\mathcal{G}}(\mathbf{s}_i) &\doteq \mathcal{I}^{\star}_{\mathrm{EQ}}(\mathbf{s}_i) - \mathcal{I}^{(n)}_{\mathrm{EQ}}(\mathbf{s}_i)\Big|_{n=1} \\ &= \mathcal{I}^{\star}_{\mathrm{EQ}}(\mathbf{s}_i) - \sum_{j \in \Psi_i} \boldsymbol{\mathcal{H}}_{i,j} - \mathbf{U}_i \end{aligned} \tag{27}$$

where $\boldsymbol{\mathcal{H}}_{i,j}$ without considering spatial information propagation is given by (20). The information gain comes from the spatial cooperation between $\mathbf{s}_i$ with its various order of connection node sets $\boldsymbol{g}_{r|i}$ $\forall\, r \in \mathbb{N}_+$.

The given analysis unveils the potential localization information inherent in network nodes connected mutually, which can improve the localization accuracy further. It is disclosed that, *the essence of spatial localization cooperation is just the spatial propagation of localization information*.

Note that the number of balance equations in (25) equals to the number of nodes inside the localization network, and their balance equations are coupled with each other. The SLIP balance states of all nodes depend not only on the node connection graph but on their own equivalent measurement information and their own *a priori* location information as well. Given a network with M nodes, the number of node connection graphs is on the order of $(M-1)^M/M!$. Hence, the closed-form solution to (25) is intractable due to the large amount of node connection situations. However, a numeric solution based on the iteration of SLIP functions in (22) ($\forall\, i = 1 : M$) is feasible. By assuming some regular properties, the SLIP analysis significantly reduces the complexity and exploits the spatial cooperation among the nodes.

B. Generic Solution

Since the amount of node connection situations is nearly exponentially growing with the number of nodes, we study a generic network case to derive the SLIP balance state, where some regular properties are assumed as follows.

- Assume $\mathbb{E}_{\mathbf{s}_i}\{\mathbf{U}_i\} = \mathbf{U}$ $\forall\, i = 1 : M$.
- Assume $\mathbb{E}_{\mathbf{s}_i,\mathbf{s}_j}\{\omega \mathbf{A}_{i,j}\} = \boldsymbol{\Lambda}$ $\forall\, j \in \Psi_i$ $\forall\, i = 1 : M$.
- Assume $|\Psi_i| = \Phi$ $\forall\, i = 1 : M$.
- Assume $\mathbb{E}_{\mathbf{s}_i}\{\mathcal{I}^{\star}_{\mathrm{BE}}(\mathbf{s}_i)\} = \boldsymbol{J}_{\star}$ $\forall\, i = 1 : M$.

[6] Here, the symbol "$\to$" denotes the direction of localization information propagation, rather than the asymptotic process under mathematical limits.

These four items indicate identical properties for all nodes, which means that, from the perspective of long-term statistical averaging, $\mathbf{U}_i$, $\mathbf{A}_{i,j}$ and connection multiplicity $|\Psi_i|$ of network node are identical to each other. That is, there is no special configuration for any node. On this basis, the associated balance equation is reformed as

$$\boldsymbol{J}_\star = \Phi\left(\boldsymbol{\Lambda}^{-1} + \boldsymbol{J}_\star^{-1}\right)^{-1} + \mathbf{U} \tag{28}$$

which can be further expressed as

$$\boldsymbol{J}_\star \boldsymbol{\Lambda}^{-1} \boldsymbol{J}_\star - \mathbf{U}\mathbf{G}\boldsymbol{J}_\star - \mathbf{U} = \mathbf{0} \tag{29}$$

where the constructed matrix $\mathbf{G}$ is given by

$$\mathbf{G} = (\Phi - 1)\mathbf{U}^{-1} + \boldsymbol{\Lambda}^{-1}. \tag{30}$$

The derivation can be found in Appendix C.

Then its balance state is obtained as

$$\boldsymbol{J}_\star = \frac{1}{2}\boldsymbol{\Lambda}^{\frac{1}{2}}\left(\boldsymbol{\Lambda}^{-\frac{1}{2}}(4\mathbf{U} + \mathbf{U}\mathbf{G}\boldsymbol{\Lambda}\mathbf{G}\mathbf{U})\boldsymbol{\Lambda}^{-\frac{1}{2}}\right)^{\frac{1}{2}}\boldsymbol{\Lambda}^{\frac{1}{2}} + \frac{1}{2}\mathbf{U}\mathbf{G}\boldsymbol{\Lambda}. \tag{31}$$

The derivation of (31) is detailed in Appendix D.

Under such generic assumptions, given the averaged *a priori* precision $\mathbf{U}$ and the averaged equivalent measurement information $\boldsymbol{\Lambda}$, the generic balance state $\boldsymbol{J}_\star$ mainly depends on the average connection multiplicity Φ of each node. Moreover, in such a generic network, the localization information gain from spatial propagation is specified as

$$\boldsymbol{\mathcal{G}} = \frac{1}{2}\boldsymbol{\Lambda}^{\frac{1}{2}}\left(\boldsymbol{\Lambda}^{-\frac{1}{2}}(4\mathbf{U} + \mathbf{U}\mathbf{G}\boldsymbol{\Lambda}\mathbf{G}\mathbf{U})\boldsymbol{\Lambda}^{-\frac{1}{2}}\right)^{\frac{1}{2}}\boldsymbol{\Lambda}^{\frac{1}{2}} - \Phi\mathbf{U}(\boldsymbol{\Lambda} + \mathbf{U})^{-1}\boldsymbol{\Lambda} + \frac{1}{2}(\Phi\boldsymbol{\Lambda} - \boldsymbol{\Lambda} - \mathbf{U}). \tag{32}$$

V. Asymptotic Analysis

Here, we aim at analyzing the asymptotic properties of spatial propagation of localization information to investigate its performance limits.

Theorem 3: The final localization accuracy of each node is upper and lower bounded as

$$\mathbf{U}_i \preceq \boldsymbol{\mathcal{I}}_{\mathrm{EQ}}^{\star}(\mathbf{s}_i) \preceq \boldsymbol{\Theta} \tag{33}$$

where the upper bound is defined as

$$\boldsymbol{\Theta} = \sum_{j\in\Psi_i} \omega\mathbf{A}_{i,j} + \mathbf{U}_i. \tag{34}$$

Proof: When the localization accuracy of all reference nodes of a generic node $\mathbf{s}_i$ is sufficiently large or arbitrarily small, based on the propagation function in (21), the localization accuracy of $\mathbf{s}_i$ becomes, respectively

$$\lim_{\substack{\boldsymbol{\mathcal{I}}_{\mathrm{EQ}}(\mathbf{s}_j)\to\infty \\ \forall\, j\in\Psi_i}} \boldsymbol{\mathcal{I}}_{\mathrm{EQ}}(\mathbf{s}_i) = \sum_{j\in\Psi_i} \omega\mathbf{A}_{i,j} + \mathbf{U}_i \doteq \boldsymbol{\Theta} \tag{35}$$

$$\lim_{\substack{\boldsymbol{\mathcal{I}}_{\mathrm{EQ}}(\mathbf{s}_j)\to\mathbf{0} \\ \forall\, j\in\Psi_i}} \boldsymbol{\mathcal{I}}_{\mathrm{EQ}}(\mathbf{s}_i) = \mathbf{U}_i \tag{36}$$

where $\boldsymbol{\mathcal{I}}_{\mathrm{EQ}}(\mathbf{s}_j) \to \boldsymbol{\infty}$ implies $\boldsymbol{\mathcal{I}}_{\mathrm{EQ}}(\mathbf{s}_j) - \mathbf{N} \succeq \mathbf{0}\ \forall\mathbf{N}$ with D-dimensions.

Due to the nondecreasing property of $\boldsymbol{\mathcal{I}}_{\mathrm{EQ}}(\mathbf{s}_i)$ with respect to its reference node location accuracy $\boldsymbol{\mathcal{I}}_{\mathrm{EQ}}(\mathbf{s}_j)$, the localization accuracy of $\mathbf{s}_i$ is bounded as

$$\mathbf{U}_i \preceq \boldsymbol{\mathcal{I}}_{\mathrm{EQ}}(\mathbf{s}_i) \preceq \boldsymbol{\Theta}. \tag{37}$$

Since the balance state $\boldsymbol{\mathcal{I}}_{\mathrm{BE}}^{\star}(\mathbf{s}_i)$ is a specific value inside the range area of localization information $\boldsymbol{\mathcal{I}}_{\mathrm{EQ}}(\mathbf{s}_i)$, thus $\boldsymbol{\mathcal{I}}_{\mathrm{EQ}}^{\star}(\mathbf{s}_i)$ is also bounded by $\mathbf{U}_i$ and $\boldsymbol{\Theta}$, as shown in (33). ■

Theorem 3 implies that the spatial localization cooperation gain $\boldsymbol{\mathcal{G}}(\mathbf{s}_i)$ defined in (27) and (30) is not more than $\boldsymbol{\Theta} - \mathbf{U}_i = \sum_{j\in\Psi_i}\omega\mathbf{A}_{i,j}$.

We now focus on analyzing the asymptotic performance of generic network localization introduced in Section V-B.

Theorem 4: The balance state $\boldsymbol{J}_\star$ of network localization accuracy is asymptotically linear with the average multiplicity Φ of network node connection, and the growth rate of final localization information $\boldsymbol{J}_\star$ with respect to node number is the averaged measurement information $\boldsymbol{\Lambda}$.

Proof: Based on (30), two involved items in (31) can be further expanded as follows:

$$\mathbf{U}\mathbf{G}\boldsymbol{\Lambda}\mathbf{G}\mathbf{U} = (\Phi - 1)^2\boldsymbol{\Lambda} + 2(\Phi - 1)\mathbf{U} + \mathbf{U}\boldsymbol{\Lambda}^{-1}\mathbf{U} \tag{38}$$

$$\mathbf{U}\mathbf{G}\boldsymbol{\Lambda} = (\Phi - 1)\boldsymbol{\Lambda} + \mathbf{U}. \tag{39}$$

Consequently, the balance state is rewritten as

$$\boldsymbol{J}_\star = \frac{\Phi - 1}{2}\boldsymbol{\Lambda}^{\frac{1}{2}}\left(\boldsymbol{\Lambda}^{-\frac{1}{2}}\left(\boldsymbol{\Lambda} + \frac{2(\Phi+1)\mathbf{U}}{(\Phi-1)^2} + \frac{\mathbf{U}\boldsymbol{\Lambda}^{-1}\mathbf{U}}{(\Phi-1)^2}\right)\boldsymbol{\Lambda}^{-\frac{1}{2}}\right)^{\frac{1}{2}} \times \boldsymbol{\Lambda}^{\frac{1}{2}} + \frac{(\Phi-1)\boldsymbol{\Lambda}}{2} + \frac{\mathbf{U}}{2}. \tag{40}$$

In addition, $\Phi^{-1}\boldsymbol{J}_\star$ reflects the equivalent information contributed from each connection node. When the averaged connection multiplicity of each node becomes very large, we have

$$\lim_{\Phi\to\infty} \Phi^{-1}\boldsymbol{J}_\star = \boldsymbol{\Lambda}. \tag{41}$$

Thus, Theorem 4 is proved. ■

Theorem 4 implies that, in a dense network case where all nodes are strongly connected to each other, the equivalent localization information contributed from one connected node is almost the averaged measurement information $\boldsymbol{\Lambda}$. Hence, the final localization accuracy of a generic node is in a level of $\Phi\boldsymbol{\Lambda}$, in cooperation with Φ connected nodes. In other words, whenever a new reference node is added for each node, there will be localization performance gain of $\boldsymbol{\Lambda}$.

Theorem 5: When the measurement precision ω is sufficiently large, we have

$$\lim_{\omega\to\infty} \boldsymbol{\mathcal{I}}_{\mathrm{EQ}}(\mathbf{s}_i) = \left(\sum_{j\in\Psi_i}\mathbf{U}_j + \mathbf{U}_i\right)^{-1}. \tag{42}$$

Theorem 5 indicates that when a sufficiently large size of measurements are sampled such that the measurement error is arbitrarily small, the localization accuracy will depend on the *a priori* precision factors only, which is independent to the geometric resolution and measurement modalities.

TABLE I
SIMULATION SETTINGS

	M	$\mathbf{V}$	$\wp$	ω
A	300	$1/500 : 1/10\mathbf{I}$	10	1
B	300	$1/100\mathbf{I}$	10	$1/7 : 1$
C	$100 : 300$	$1/100\mathbf{I}$	10	1
D	300	$1/100\mathbf{I}$	10	1

VI. NUMERICAL RESULTS

We now present extensive simulation results to validate the spatial propagation analysis in this paper.

A. Simulation Setting

In order to configure the *a priori* location precision of network node in the simulations, we assume that it complies with a Wishart distribution, namely, $\mathbf{U}_i \sim \mathcal{W}(\mathbf{U}_i|\mathbf{V}, \wp)\ \forall\, i = 1 : M$, where $\mathbf{V}$ denotes the scaling matrix, and $\wp$ stands for the associated degree of freedom. The reason of employing Wishart distribution lies in the fact that it is commonly used to model the precision parameter of a Gaussian distribution and it is also the conjugate *a priori* of the Gaussian distribution precision [32]. Consequently, we can see that, the averaged *a priori* precision of the network node locations is $\wp\mathbf{V}$, which can reflect the level of location uncertainties of network nodes. We use the matrix trace as the metric to assess the localization accuracy or error since we consider the fact that it is the trace of equivalent CRLB that acts upon the mean squared localization errors, namely, $\mathrm{tr}(\boldsymbol{\mathcal{B}}_{\mathrm{EQ}}(\mathbf{s}_i)) \leq \mathrm{cov}(\widehat{\mathbf{s}}_i)$, where we define $\boldsymbol{\mathcal{B}}_{\mathrm{EQ}}(\mathbf{s}_i) = (\boldsymbol{\mathcal{I}}_{\mathrm{EQ}}(\mathbf{s}_i))^{-1}$. All results are averaged over a total of 1000 simulation runs.

Here, we consider the RSS-based network localization in an area of 100[m] $\times$ 100[m]. We also assume that $\gamma = 3$, $P_T = 50$, $L_0 = 1$, $d_0 = 1$, and $r_s = 20\,[\mathrm{m}]$ throughout the simulations. To clearly demonstrate the spatial propagation behavior of localization information (or errors) in different environments, we first simulate Scenarios A, B, and C here. The simulation settings are summarized in Table I. Furthermore, Scenario D is simulated to examine the details of spatial propagation.

B. Simulation Results

The convergence behavior of spatial propagation of the localization information in different environments (i.e., scenarios A, B, and C) are shown in Fig. 5, and its localization EP convergence is correspondingly shown in Fig. 6, wherein those three subfigures correspond to Scenarios A, B and C, respectively.

As shown in Figs. 5 and 6, the localization of all network nodes benefits from the spatial propagation of corresponding localization information (see more details in Fig. 7). Through spatial cooperation, all node location precision approaches up to the associated balance state. In addition, in terms of mean squared localization errors, the network localization with less *a priori* location information and larger measurement information benefits more from the spatial cooperation, as shown in Fig. 6.

We examine the localization performance bounds (see Theorem 3) and the localization performance gain over scenario D in Table I. As shown in Fig. 7, the localization information $\boldsymbol{\mathcal{I}}_{\mathrm{EQ}}(\mathbf{s}_i)$ (as well as its balance state $\boldsymbol{\mathcal{I}}^{\star}_{\mathrm{EQ}}(\mathbf{s}_i)$) is upper and lower bounded by $\boldsymbol{\Theta}$ and $\mathbf{U}_i$, respectively. However, due to the limited final localization accuracy $\boldsymbol{\mathcal{I}}^{\star}_{\mathrm{EQ}}(\mathbf{s}_j)$ of reference node $\mathbf{s}_j$ $(\forall\, j \in \Psi_i)$, there still exists a gap between $\boldsymbol{\mathcal{I}}^{\star}_{\mathrm{EQ}}(\mathbf{s}_i)$ with its upper bound $\boldsymbol{\Theta}$.

Moreover, as shown in Fig. 7, the localization information at the first round of propagation (i.e., $n=1$) denotes the performance of traditional cooperative localization schemes, where there is localization cooperation only between a node and its nearby nodes. While when $n \geq 2$, the localization information of a node can be further leveled up due to the spatial cooperation with its remote nodes. Hence, benefiting from spatial propagation, the network localization reap more localization cooperation gain $\boldsymbol{\mathcal{G}}(\mathbf{s}_i)$ from its various order of connection node set $\boldsymbol{g}_{r|i}$ $\forall\, r \in \mathbb{N}_+$.

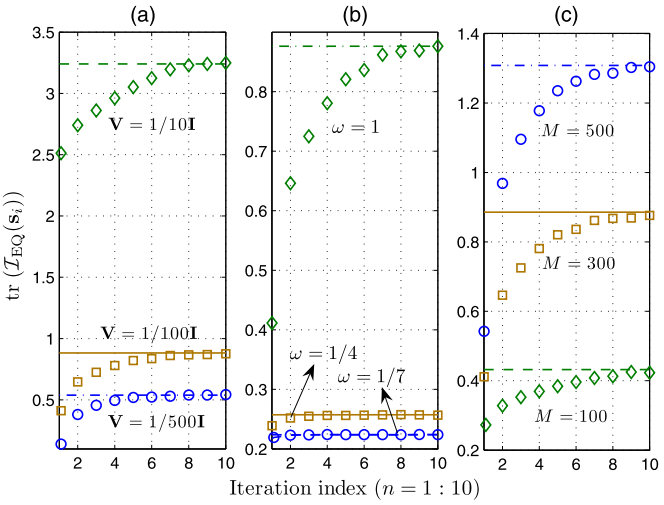

Fig. 5. Spatial propagation convergence of the localization information. The discontinuous curves stand for the localization information $\boldsymbol{\mathcal{I}}^{(n)}_{\mathrm{EQ}}(\mathbf{s}_i)$, whereas the horizontal lines correspond to the associated balance states $\boldsymbol{\mathcal{I}}^{\star}_{\mathrm{EQ}}(\mathbf{s}_i)$. In particular, at the first round of localization (namely $n = 1$), $\boldsymbol{\mathcal{I}}_{\mathrm{EQ}}(\mathbf{s}_i)$ corresponds to the localization information without spatial information propagation, wherein the location information that each reference node $\mathbf{s}_j$ $(\forall\, j \in \Psi_i)$ propagates to the objective node $\mathbf{s}_i$ is its original *a priori* $\mathbf{U}_j$ only. However, from the iterations of $n \geq 2$, the cooperative localization begins to benefit from the spatial propagation of localization information among network nodes. Gradually, the network localization information converges to a higher level and maintains balance, as unveiled in Theorem 2.

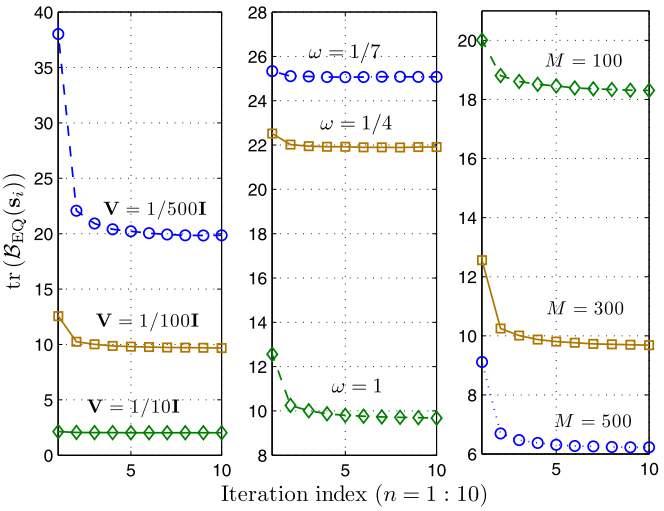

Fig. 6. Spatial propagation convergence of the localization errors.

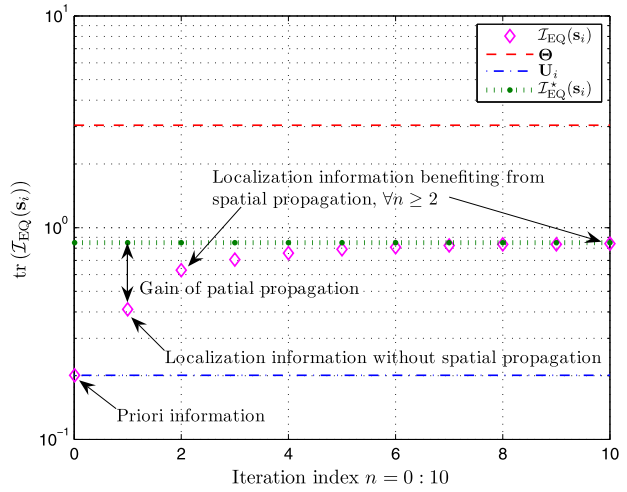

Fig. 7. Information gain inside spatial localization propagation.

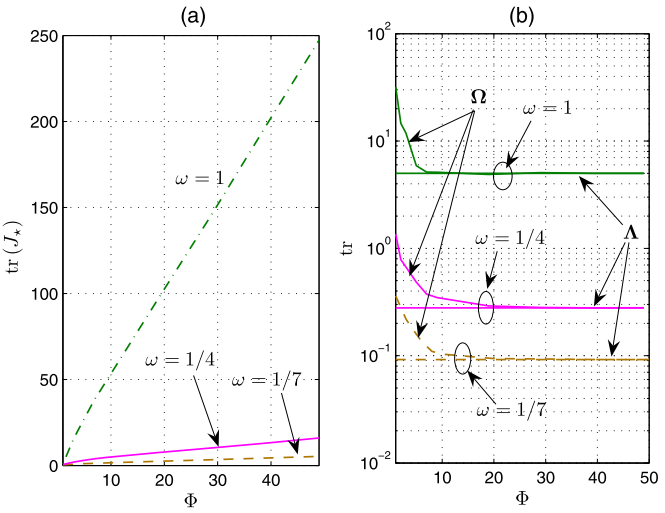

Fig. 8. Balanced localization information $\boldsymbol{J}_\star$ and its growth rate $\mathbf{\Omega}$ under different connection multiplicities Φ and different environments. The growth rate is defined as $\mathbf{\Omega} \doteq \boldsymbol{J}_\star(\Phi) - \boldsymbol{J}_\star(\Phi-1)$, where the balance state $\boldsymbol{J}_\star(\Phi)$ is regarded as a function of the averaged connection multiplicity Φ. The growth rate $\mathbf{\Omega}$ reflects the localization information contributed by one node.

Fig. 8(a) and (b) present the balanced localization information $\boldsymbol{J}_\star$ (in a generic case considered in Section IV-B) and its growth rate $\mathbf{\Omega}$ in different environments, where we set $\mathbf{V} = 1/100\mathbf{I}$ and $\wp = 10$, whereas the measurement precision ω varies in [1/7,1]. In particular, the averaged connection multiplicity Φ of each node is set to rang from 1 to 49 to unveil its localization information. We can see from Fig. 8(a) that $\boldsymbol{J}_\star(\Phi)$ is asymptotically linear with the connection multiplicity Φ, as unveiled in Theorem 4. This conclusion can also be observed from Fig. 8(b), where the corresponding growth rate $\mathbf{\Omega}$ converges to a lower value $\mathbf{\Lambda}$.

VII. Concluding Remarks

In this paper, the fundamental limits and spatial cooperation of wireless network localization have been studied. It is shown that the localization accuracy depends on the measurement size, the density of independent reference sources, *a priori* information of node location, the geometric resolution of measurement methodology, and the measurement noise intensity. In addition, a remote node can contribute to the localization of another node through spatial propagation of the localization information if there is a measurement-connection link between them. It is revealed that the essence of spatial localization cooperation is the spatial propagation of localization information factors. Given a fixed size of network measurements, the node location accuracy will converge statistically to a higher level through spatial localization cooperation, although the initial locations of the reference nodes are inaccurate. In addition, we have the following conclusions.

- The network localization EP principle complies with Ohm's law in electric circuit theory, where the measurement accuracy, node location accuracy, and measurement-resolution information behave similarly to the resistances connected in parallel or series.
- In a dense network, for the localization of a generic node, the localization information contribution from one of its reference nodes is almost the averaged measurement information $\mathbf{\Lambda}$. Hence, the localization accuracy of a node, in cooperation with its Φ reference nodes, is $\Phi\mathbf{\Lambda}$.
- If the measurement size is sufficiently large, the localization accuracy will depend on the *a priori* precision factors only, which is independent of the geometric resolution and measurement methodologies.

Furthermore, a generic balance state of spatial propagation of network localization information is derived in this paper, as well as its upper and lower bounds, which corresponds to the ultimate performance limits of cooperative localization with a fixed size of measurements. The spatial information propagation analysis in this paper can be applied to the TOA, AOA, and RSS-based localization.

The spatial information propagation associated with simultaneous localization and tracking will be interesting problems to be investigated in the future.

Appendix A
Derivation of (20)

Given two squared and invertible matrices $\mathbf{A}$ and $\mathbf{X}$, the inverse matrix lemma is described as follows:

$$(\mathbf{A}+\mathbf{X})^{-1} = \mathbf{A}^{-1} - \left(\mathbf{A}^{\top}\mathbf{X}^{-1}\mathbf{A} + \mathbf{A}\right)^{-1}. \tag{43}$$

Based on the given lemma, we have that

$$(\omega\mathbf{A}_{i,j} + \mathbf{U}_j)^{-1} = (\omega\mathbf{A}_{i,j})^{-1} - \left(\omega^2\mathbf{A}_{i,j}^{\top}\mathbf{U}_j^{-1}\mathbf{A}_{i,j} + \omega\mathbf{A}_{i,j}\right)^{-1}. \tag{44}$$

Note that $\mathbf{A}_{i,j}$ and $\mathbf{U}_j$ are symmetric and have full rank. Hence, $\mathbf{\Phi}_{\rm BE}^{\top}(\mathbf{s}_i)(\boldsymbol{\mathcal{R}}_{\rm BE}(\mathbf{s}_i))^{-1}\mathbf{\Phi}_{\rm BE}(\mathbf{s}_i)$ can be specified as

$$\begin{aligned}
&\sum_{j\in\Psi_i} \omega^2\mathbf{A}_{i,j}^{\top}(\omega\mathbf{A}_{i,j} + \mathbf{U}_j)^{-1}\mathbf{A}_{i,j} \\
&= \sum_{j\in\Psi_i} \omega\mathbf{A}_{i,j}^{\top} - \sum_{j\in\Psi_i} \omega\mathbf{A}_{i,j}^{\top}\left(\omega\mathbf{A}_{i,j}^{\top}\mathbf{U}_j^{-1}\mathbf{A}_{i,j} + \mathbf{A}_{i,j}\right)^{-1}\mathbf{A}_{i,j} \\
&= \sum_{j\in\Psi_i} \omega\mathbf{A}_{i,j}^{\top} - \sum_{j\in\Psi_i} \left((\omega\mathbf{A}_{i,j})^{-1} + \mathbf{U}_j^{-1}\right)^{-1}.
\end{aligned} \tag{45}$$

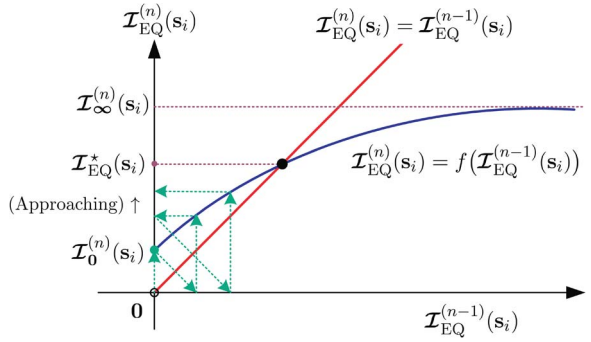

Fig. 9. Rough graph of the SLIP function $\mathcal{I}_{\mathrm{EQ}}^{(n)}(\mathbf{s}_i)=f(\mathcal{I}_{\mathrm{EQ}}^{(n-1)}(\mathbf{s}_i))$.

Hence, the equivalent localization information $\mathcal{I}_{\mathrm{EQ}}(\mathbf{s}_i)$ can be finally expressed as (20).

Appendix B
Proof of Theorem 2

As indicated in (22), the current localization information $\mathcal{I}_{\mathrm{EQ}}^{(n)}(\mathbf{s}_i)$ can be read as a function of its last state $\mathcal{I}_{\mathrm{EQ}}^{(n-1)}(\mathbf{s}_i)$, namely, $\mathcal{I}_{\mathrm{EQ}}^{(n)}(\mathbf{s}_i) = f(\mathcal{I}_{\mathrm{EQ}}^{(n-1)}(\mathbf{s}_i))$. Based on (22), when $\mathcal{I}_{\mathrm{EQ}}^{(n-1)}(\mathbf{s}_i)\to\boldsymbol{\infty}$ and $\mathcal{I}_{\mathrm{EQ}}^{(n-1)}(\mathbf{s}_i)\to\mathbf{0}$, the localization information of the next step follows (46) and (47), respectively, shown at the bottom of the page. Here, $\mathcal{I}_{\mathrm{EQ}}^{(n-1)}(\mathbf{s}_i)\to\boldsymbol{\infty}$ means $\mathcal{I}_{\mathrm{EQ}}^{(n-1)}(\mathbf{s}_i) - \mathbf{M} \succeq \mathbf{0}, \forall \mathbf{M} \succeq \mathbf{0}$. Moreover, we have $\mathbf{0} \preceq \mathcal{I}_{\mathbf{0}}^{(n)}(\mathbf{s}_i) \preceq \mathcal{I}_{\boldsymbol{\infty}}^{(n)}(\mathbf{s}_i) \prec \boldsymbol{\infty}$. Meanwhile, the SLIP function $\mathcal{I}_{\mathrm{EQ}}^{(n)}(\mathbf{s}_i)=f(\mathcal{I}_{\mathrm{EQ}}^{(n-1)}(\mathbf{s}_i))$ is monotonously increasing. In brief, the properties of SLIP are summarized as follows.

- $\mathcal{I}_{\mathrm{EQ}}^{(n)}(\mathbf{s}_i)=f(\mathcal{I}_{\mathrm{EQ}}^{(n-1)}(\mathbf{s}_i))$ is monotonously increasing.
- $\mathbf{0}\preceq\mathcal{I}_{\mathbf{0}}^{(n)}(\mathbf{s}_i)\preceq\mathcal{I}_{\boldsymbol{\infty}}^{(n)}(\mathbf{s}_i)\prec\boldsymbol{\infty}$.

Consequently, there must be one and only one intersection (denoted by $\mathcal{I}_{\mathrm{EQ}}^{\star}(\mathbf{s}_i)$) Between $\mathcal{I}_{\mathrm{EQ}}^{(n)}(\mathbf{s}_i)=f(\mathcal{I}_{\mathrm{EQ}}^{(n-1)}(\mathbf{s}_i))$ and $\mathcal{I}_{\mathrm{EQ}}^{(n)}(\mathbf{s}_i)=\mathcal{I}_{\mathrm{EQ}}^{(n-1)}(\mathbf{s}_i)$, as roughly shown in Fig. 9.

At the beginning of SLIP (suppose $n=0$), since there is no *a posteriori* information about $\mathbf{s}_i$; thus, $\mathcal{I}_{\mathrm{EQ}}^{(0)}(\mathbf{s}_i)=\mathbf{0}$. Next, with the progress of SLIP ($n=1,2,\ldots$), the localization information $\mathcal{I}_{\mathrm{EQ}}^{(n)}(\mathbf{s}_i)$ gradually increases and approaches the intersection $\mathcal{I}_{\mathrm{EQ}}^{\star}(\mathbf{s}_i)$ from the left side. Suppose there is a situation that the present localization information $\mathcal{I}_{\mathrm{EQ}}^{(n)}(\mathbf{s}_i)$ grows up such that it exceeds $\mathcal{I}_{\mathrm{EQ}}^{\star}(\mathbf{s}_i)$. Then, at the next propagation step, $\mathcal{I}_{\mathrm{EQ}}^{(n+1)}(\mathbf{s}_i)$ will become lower than $\mathcal{I}_{\mathrm{EQ}}^{(n)}(\mathbf{s}_i)$ since we have $\mathcal{I}_{\mathrm{EQ}}^{(n)}(\mathbf{s}_i)\prec\mathcal{I}_{\mathrm{EQ}}^{(n-1)}(\mathbf{s}_i)$ when $\mathcal{I}_{\mathrm{EQ}}^{(n)}(\mathbf{s}_i)\succ\mathcal{I}_{\mathrm{EQ}}^{\star}(\mathbf{s}_i)$, according to SLIP properties, as also shown in Fig. 9.

In a word, the localization information will gradually level up to $\mathcal{I}_{\mathrm{EQ}}^{\star}(\mathbf{s}_i)$ and then keep balance until there is more measurement input. Hence, Theorem 2 is proved.

Appendix C
Derivation of (29)

Since the equation $(\boldsymbol{\Lambda}^{-1}+\boldsymbol{J}_{\star}^{-1})^{-1}=\boldsymbol{J}_{\star}(\boldsymbol{\Lambda}+\boldsymbol{J}_{\star})^{-1}\boldsymbol{\Lambda}$ holds, (28) can be equivalently expressed as follows:

$$\boldsymbol{J}_{\star}=\Phi\boldsymbol{J}_{\star}(\boldsymbol{\Lambda}+\boldsymbol{J}_{\star})^{-1}\boldsymbol{\Lambda}+\mathbf{U} \tag{48}$$

$$\boldsymbol{J}_{\star}\boldsymbol{\Lambda}^{-1}(\boldsymbol{\Lambda}+\boldsymbol{J}_{\star})=\Phi\boldsymbol{J}_{\star}+\mathbf{U}\boldsymbol{\Lambda}^{-1}(\boldsymbol{\Lambda}+\boldsymbol{J}_{\star}) \tag{49}$$

$$\boldsymbol{J}_{\star}\boldsymbol{\Lambda}^{-1}\boldsymbol{J}_{\star}+\boldsymbol{J}_{\star}=\Phi\boldsymbol{J}_{\star}+\mathbf{U}+\mathbf{U}\boldsymbol{\Lambda}^{-1}\boldsymbol{J}_{\star}. \tag{50}$$

Hence, the balance equation can be further cast as

$$\boldsymbol{J}_{\star}\boldsymbol{\Lambda}^{-1}\boldsymbol{J}_{\star}-\mathbf{U}\left(\underbrace{(\Phi-1)\mathbf{U}^{-1}+\boldsymbol{\Lambda}^{-1}}_{\mathbf{G}}\right)\boldsymbol{J}_{\star}-\mathbf{U}=\mathbf{0}. \tag{51}$$

Consequently, (29) is obtained.

Appendix D
Derivation of (31)

At first, we give two conclusions below, which are useful for deriving the balance state $\boldsymbol{J}_{\star}$

$$\mathbf{U}\mathbf{G}\boldsymbol{J}_{\star}=\boldsymbol{J}_{\star}\mathbf{G}\mathbf{U} \tag{52}$$

$$\boldsymbol{\Lambda}^{-\frac{1}{2}}\mathbf{U}\mathbf{G}\boldsymbol{\Lambda}^{\frac{1}{2}}=\boldsymbol{\Lambda}^{\frac{1}{2}}\mathbf{G}\mathbf{U}\boldsymbol{\Lambda}^{-\frac{1}{2}}. \tag{53}$$

Based on the fact $\mathbf{G}=(\Phi-1)\mathbf{U}^{-1}+\boldsymbol{\Lambda}^{-1}$, (53) can be directly proved. The balance state $\boldsymbol{J}_{\star}$ meets with (52), which will be proved in Appendix E.

Consequently, based on (29), we have (54)–(58), shown at the top of the next page, where (55) and (57) have used the results shown in (52) and (53), respectively. Moreover, the balance equation can be further derived as

$$\boldsymbol{\Lambda}^{-\frac{1}{2}}\boldsymbol{J}_{\star}\boldsymbol{\Lambda}^{-\frac{1}{2}}=\frac{1}{2}\left(4\boldsymbol{\Lambda}^{-\frac{1}{2}}\mathbf{U}\boldsymbol{\Lambda}^{-\frac{1}{2}}+\boldsymbol{\Lambda}^{-\frac{1}{2}}\mathbf{U}\mathbf{G}\boldsymbol{\Lambda}\mathbf{G}\mathbf{U}\boldsymbol{\Lambda}^{-\frac{1}{2}}\right)^{\frac{1}{2}}+\frac{1}{2}\boldsymbol{\Lambda}^{-\frac{1}{2}}\mathbf{U}\mathbf{G}\boldsymbol{\Lambda}^{\frac{1}{2}}. \tag{59}$$

By premultiplying and postmultiplying $\boldsymbol{\Lambda}^{1/2}$ at both sides of (59), the balance state in (31) is thus obtained.

$$\lim_{\mathcal{I}_{\mathrm{EQ}}^{(n-1)}(\mathbf{s}_i)\to\boldsymbol{\infty}}\mathcal{I}_{\mathrm{EQ}}^{(n)}(\mathbf{s}_i)=\sum_{j\in\Psi_i}\left((\omega\mathbf{A}_{i,j})^{-1}+\left(\sum_{k\in\Psi_j\backslash i}\boldsymbol{\mathcal{H}}_{j,k}^{(n)}+\omega\mathbf{A}_{j,i}+\mathbf{U}_j\right)^{-1}\right)^{-1}+\mathbf{U}_i\doteq\mathcal{I}_{\boldsymbol{\infty}}^{(n)}(\mathbf{s}_i) \tag{46}$$

$$\lim_{\mathcal{I}_{\mathrm{EQ}}^{(n-1)}(\mathbf{s}_i)\to\mathbf{0}}\mathcal{I}_{\mathrm{EQ}}^{(n)}(\mathbf{s}_i)=\sum_{j\in\Psi_i}\left((\omega\mathbf{A}_{i,j})^{-1}+\left(\sum_{k\in\Psi_j\backslash i}\boldsymbol{\mathcal{H}}_{j,k}^{(n)}+\mathbf{U}_j\right)^{-1}\right)^{-1}+\mathbf{U}_i\doteq\mathcal{I}_{\mathbf{0}}^{(n)}(\mathbf{s}_i) \tag{47}$$

$$\boldsymbol{J}_\star \boldsymbol{\Lambda}^{-1} \boldsymbol{J}_\star - \mathbf{U}\mathbf{G}\boldsymbol{J}_\star = \mathbf{U} \tag{54}$$

$$\left(\boldsymbol{J}_\star \boldsymbol{\Lambda}^{-\frac{1}{2}} - \frac{1}{2}\mathbf{U}\mathbf{G}\boldsymbol{\Lambda}^{\frac{1}{2}}\right)\left(\boldsymbol{\Lambda}^{-\frac{1}{2}}\boldsymbol{J}_\star - \frac{1}{2}\boldsymbol{\Lambda}^{\frac{1}{2}}\mathbf{G}\mathbf{U}\right) = \mathbf{U} + \frac{1}{4}\mathbf{U}\mathbf{G}\boldsymbol{\Lambda}\mathbf{G}\mathbf{U}\Big|_{\text{employing Eq.(52)}} \tag{55}$$

$$\left(\boldsymbol{\Lambda}^{-\frac{1}{2}}\boldsymbol{J}_\star\boldsymbol{\Lambda}^{-\frac{1}{2}} - \frac{1}{2}\boldsymbol{\Lambda}^{-\frac{1}{2}}\mathbf{U}\mathbf{G}\boldsymbol{\Lambda}^{\frac{1}{2}}\right)\left(\boldsymbol{\Lambda}^{-\frac{1}{2}}\boldsymbol{J}_\star\boldsymbol{\Lambda}^{-\frac{1}{2}} - \frac{1}{2}\boldsymbol{\Lambda}^{\frac{1}{2}}\mathbf{G}\mathbf{U}\boldsymbol{\Lambda}^{-\frac{1}{2}}\right) = \boldsymbol{\Lambda}^{-\frac{1}{2}}\mathbf{U}\boldsymbol{\Lambda}^{-\frac{1}{2}} + \frac{1}{4}\boldsymbol{\Lambda}^{-\frac{1}{2}}\mathbf{U}\mathbf{G}\boldsymbol{\Lambda}\mathbf{G}\mathbf{U}\boldsymbol{\Lambda}^{-\frac{1}{2}} \tag{56}$$

$$\left(\boldsymbol{\Lambda}^{-\frac{1}{2}}\boldsymbol{J}_\star\boldsymbol{\Lambda}^{-\frac{1}{2}} - \frac{1}{2}\boldsymbol{\Lambda}^{-\frac{1}{2}}\mathbf{U}\mathbf{G}\boldsymbol{\Lambda}^{\frac{1}{2}}\right)^2 = \boldsymbol{\Lambda}^{-\frac{1}{2}}\mathbf{U}\boldsymbol{\Lambda}^{-\frac{1}{2}} + \frac{1}{4}\boldsymbol{\Lambda}^{-\frac{1}{2}}\mathbf{U}\mathbf{G}\boldsymbol{\Lambda}\mathbf{G}\mathbf{U}\boldsymbol{\Lambda}^{-\frac{1}{2}}\Big|_{\text{using (53)}} \tag{57}$$

$$\boldsymbol{\Lambda}^{-\frac{1}{2}}\boldsymbol{J}_\star\boldsymbol{\Lambda}^{-\frac{1}{2}} - \frac{1}{2}\boldsymbol{\Lambda}^{-\frac{1}{2}}\mathbf{U}\mathbf{G}\boldsymbol{\Lambda}^{\frac{1}{2}} = \left(\boldsymbol{\Lambda}^{-\frac{1}{2}}\mathbf{U}\boldsymbol{\Lambda}^{-\frac{1}{2}} + \frac{1}{4}\boldsymbol{\Lambda}^{-\frac{1}{2}}\mathbf{U}\mathbf{G}\boldsymbol{\Lambda}\mathbf{G}\mathbf{U}\boldsymbol{\Lambda}^{-\frac{1}{2}}\right)^{\frac{1}{2}} \tag{58}$$

APPENDIX E
DERIVATION OF (52)

Since $(\boldsymbol{\Lambda}^{-1} + \boldsymbol{J}_\star^{-1})^{-1} = \boldsymbol{\Lambda}(\boldsymbol{\Lambda} + \boldsymbol{J}_\star)^{-1}\boldsymbol{J}_\star$ also holds, (28) can be rewritten as

$$\boldsymbol{J}_\star = \Phi\boldsymbol{\Lambda}(\boldsymbol{\Lambda} + \boldsymbol{J}_\star)^{-1}\boldsymbol{J}_\star + \mathbf{U}. \tag{60}$$

By doing similar manipulations with (49) and (50), (28) can also be expressed as

$$\boldsymbol{J}_\star\boldsymbol{\Lambda}^{-1}\boldsymbol{J}_\star - \boldsymbol{J}_\star\mathbf{G}\mathbf{U} - \mathbf{U} = \mathbf{0}. \tag{61}$$

Combining with (51), we can see that the balance state meets with (52), namely, $\mathbf{U}\mathbf{G}\boldsymbol{J}_\star = \boldsymbol{J}_\star\mathbf{G}\mathbf{U}$.

REFERENCES

[1] M. D. Dikaiakos, A. Florides, T. Nadeem, and L. Iftode, "Location-aware services over vehicular ad-hoc networks using car-to-car communication," *IEEE J. Sel. Areas Commun.*, vol. 25, no. 8, pp. 1590–1602, Oct. 2007.

[2] Y. Cao *et al.*, "Geographic-Based Spray-and-Relay (GSaR): An efficient routing scheme for DTNs," *IEEE Trans. Veh. Technol.*, vol. 64, no. 4, pp. 1548–1564, Apr. 2015.

[3] Y. Cao, H. Cruickshank, and Z. Sun, "A routing framework for delay tolerant networks based on encounter angle," in *Proc. 7th IWCMC*, Jul. 4–8, 2011, pp. 2231–2236.

[4] E. Kaasinen, "User needs for location-aware mobile services," *Pers. Ubiquitous Comput.*, vol. 7, no. 1, pp. 70–79, May 2003.

[5] M. Li *et al.*, "All your location are belong to us: Breaking mobile social networks for automated user location tracking," in *Proc. MobiHoc*, 2014, pp. 43–52.

[6] H. Li, L. Sun, H. Zhu, X. Lu, and X. Cheng, "Achieving privacy preservation in WiFi fingerprint-based localization," in *Proc. IEEE INFOCOM*, Apr. 27–May 2, 2014, pp. 2337–2345.

[7] S. M. Kay, *Fundamentals of Statistical Signal Processing, Volume 2: Detection Theory*. Englewood Cliffs, NJ, USA: Prentice-Hall, 1998.

[8] P. Lamon, I. Nourbakhsh, B. Jensen, and R. Siegwart, "Deriving and matching image fingerprint sequences for mobile robot localization," in *Proc. ICRA*, May 2001, pp. 1609–1614.

[9] G. Schroth *et al.*, "Mobile visual location recognition," *IEEE Signal Process. Mag.*, vol. 28, no. 4, pp. 77–89, Jul. 2011.

[10] X. Sheng and Y. Hu, "Maximum likelihood multiple-source localization using acoustic energy measurements with wireless sensor networks," *IEEE Trans. Signal Process.*, vol. 53, no. 1, pp. 44–53, Jan. 2005.

[11] G. Sun, J. Chen, W. Guo, and K. Liu, "Signal processing techniques in network-aided positioning: A survey of state-of-the-art positioning designs," *IEEE Signal Process. Mag.*, vol. 22, no. 4, pp. 12–23, Jul. 2005.

[12] Z. Yang, Z. Zhou, and Y. Liu, "From RSSI to CSI: Indoor localization via channel response," *ACM Comput. Surv.*, vol. 46, no. 2, pp. 1–32, Nov. 2013.

[13] S. Jung, S. Hann, and C. Park, "TDOA-based optical wireless indoor localization using LED ceiling lamps," *IEEE Trans. Consum. Electron.*, vol. 57, no. 4, pp. 1592–1597, Nov. 2011.

[14] Y. Shen and M. Z. Win, "Fundamental limits of wideband localization-Part I: A general framework," *IEEE Trans. Inf. Theory*, vol. 56, no. 10, pp. 4956–4979, Oct. 2010.

[15] Y. Shen, H. Wymeersch, and M. Z. Win, "Fundamental limits of wideband localization-Part II: Cooperative networks," *IEEE Trans. Inf. Theory*, vol. 56, no. 10, pp. 4981–5000, Oct. 2010.

[16] M. Z. Win *et al.*, "Network localization and navigation via cooperation," *IEEE Commun. Mag.*, vol. 49, no. 5, pp. 56–62, May 2011.

[17] J. Teng, H. Snoussi, C. Richard, and R. Zhou, "Distributed variational filtering for simultaneous sensor localization and target tracking in wireless sensor networks," *IEEE Trans. Veh. Technol.*, vol. 61, no. 5, pp. 2305–2318, Jun. 2012.

[18] B. Hao, "On the Cramer–Rao bound of multiple sources localization using RDOAs and GROAs in the presence of sensor location uncertainties," in *Proc. IEEE WCNC*, 2012, pp. 3117–3122.

[19] S. Mazuelas, Y. Shen, and M. Z. Win, "Information coupling in cooperative localization," *IEEE Commun. Lett.*, vol. 15, no. 7, pp. 737–739, Jul. 2011.

[20] Y. Shen, S. Mazuelas, and M. Z. Win, "Network navigation: Theory and interpretation," *IEEE J. Sel. Areas Commun.*, vol. 30, no. 9, pp. 1823–1834, Oct. 2012.

[21] F. Gustafsson and F. Gunnarsson, "Mobile positioning using wireless networks: Possibilities and fundamental limitations based on available wireless network measurements," *IEEE Signal Process. Mag.*, vol. 22, no. 4, pp. 41–53, Jul. 2005.

[22] M. Angjelichinoski, D. Denkovski, V. Atanasovski, and L. Gavrilovska, "Cramér–Rao lower bounds of RSS-based localization with anchor position uncertainty," *IEEE Trans. Inf. Theory*, vol. 61, no. 5, pp. 2807–2834, May 2015.

[23] I. Sharp, K. Yu, and T. Sathyan, "Positional accuracy measurement and error modeling for mobile tracking," *IEEE Trans. Mobile Comput.*, vol. 11, no. 6, pp. 1021–1032, Jun. 2012.

[24] I. Güvenç, C. C. Chong, F. Watanabe, and H. Inamura, "NLOS identification and weighted least-squares localization for UWB systems using multipath channel statistics," *EURASIP J. Adv. Signal Process.*, vol. 2008, Jan. 2008, Art. no. 271984.

[25] A. Conti, M. Guerra, D. Dardari, N. Decarli, and M. Z. Win, "Network experimentation for cooperative localization," *IEEE J. Sel. Areas Commun.*, vol. 30, no. 2, pp. 467–475, Feb. 2012.

[26] I. Güvenç and C. C. Chong, "A survey on TOA based wireless localization and NLOS mitigation techniques," *IEEE Commun. Surveys Tuts.*, vol. 11, no. 3, pp. 107–124, 3rd Quart. 2009.

[27] G. Giorgetti, S. K. Gupta, and G. Manes, "Understanding the limits of RF-based collaborative localization," *IEEE/ACM Trans. Netw.*, vol. 19, no. 6, pp. 1638–1651, Dec. 2011.

[28] R. W. Ouyang, A. K.-S. Wong, and C.-T. Lea, "Received signal strength-based wireless localization via semidefinite programming: Noncooperative and cooperative schemes," *IEEE Trans. Veh. Technol.*, vol. 59, no. 3, pp. 1307–1318, Mar. 2010.

[29] P. Rong and M. L. Sichitiu, "Angle of arrival localization for wireless sensor networks," in *Proc. 3rd Annu. IEEE Commun. SECON*, 2006, pp. 374–382.

[30] J. Xu, M. Ma, and C. L. Law, "Cooperative angle-of-arrival position localization," *Measurement*, vol. 59, pp. 302–313, 2015.
[31] P. M. Djuric, M. V. Vemula, M. R. Bugallo, and J. Miguez, "Non-cooperative localization of binary sensors," in *Proc. IEEE 13th Workshop Statist. Signal Process.*, 2005, pp. 1244–1249.
[32] Y. Dodge, *The Oxford Dictionary of Statistical Terms*. London, U.K.: Oxford Univ. Press, 2003.

Bingpeng Zhou received the B.E. degree in electronic and information engineering from Zhongyuan University of Technology, Zhengzhou, China, in 2010. He is currently working toward the Ph.D. degree with the School of Information Science and Technology, Southwest Jiaotong University, Chengdu, China.

From September to November 2015, he was a Visiting Ph.D. Student with the 5G Innovation Centre, University of Surrey, Guildford, U.K. His current research interests include wireless localization and tracking, distributed Bayesian inference and filtering, machine learning, and wireless fast-time-varying communication systems.

Qingchun Chen (M'06–SM'14) received the B.Sc. and M.Sc. degrees (with Hons.) from Chongqing University, Chongqing, China, in 1994 and 1997, respectively, and the Ph.D. degree from Southwest Jiaotong University, Chengdu, China, in 2004.

Since 2004, he has been with Southwest Jiaotong University, first as an Associate Professor and then as a Full Professor since 2009. He is the author and coauthor of more than 80 research papers, two book chapters, and 20 patents. His research interests include wireless communication, wireless network, channel coding, and signal processing.

Dr. Chen currently serves as an Associate Editor for IEEE ACCESS.

Pei Xiao (SM'11) received the Ph.D. degree from Chalmers University of Technology, Gothenburg, Sweden, in 2004.

He was a Research Fellow with Queen's University Belfast, Belfast, U.K. and had held positions with Nokia Networks, Finland. Since 2011, he has been with the University of Surrey, Guildford, U.K., where he is currently a Reader and the Technical Manager of the 5G Innovation Centre (5GIC), leading and coordinating research activities in all the work areas in 5GIC. His research interests include a wide range of areas in communications theory and signal processing for wireless communications.

Lian Zhao (S'99–M'03–SM'06) received the Ph.D. degree from the University of Waterloo, Waterloo, ON, Canada, in 2002.

Since 2003, she has been with the Department of Electrical and Computer Engineering (ELCE), Ryerson University, Toronto, ON, first as an Assistant Professor, then as an Associate Professor (2007), and, currently, as a Professor. Since 2013, she has been the Program Director for Graduate Studies with ELCE, Ryerson University. Her research interests include wireless communications, radio resource management, power control, cognitive radio and cooperative communications, and the design and applications of the energy-efficient wireless sensor networks.

Dr. Zhao has served as the IEEE Ryerson Student Branch Counselor since 2005, the Web Conference Cochair for the 2009 IEEE Toronto International Conference Science and Technology for Humanity, the Symposium Cochair for the 2013 IEEE Global Communications Conference Communication Theory Symposium, and a technical program committee member for numerous IEEE flagship conferences. She served as a Guest Editor for the *International Journal on Communication Networks and Distributed Systems*, Special Issue on Cognitive Radio Networks in 2011, as an Associate Editor for the IEEE TRANSACTIONS ON VEHICULAR TECHNOLOGY since 2013, and as a Reviewer for IEEE TRANSACTIONS and for various Natural Sciences and Engineering Research Council proposals. She received the Canada Foundation for Innovation New Opportunity Research Award in 2005; the Ryerson Faculty Merit Award in 2005 and 2007; the Faculty Research Excellence Award from ELCE, Ryerson University, in 2010 and 2012; the Best Student Paper Award (with her student) from the EAI International Conference on Communications and Networking in China in 2011; and the Best Paper Award (with her student) from the 2013 International Conference on Wireless Communications and Signal Processing. She is a licensed Professional Engineer in Ontario and a member of the IEEE Communication and Vehicular Societies.